Molecular Biology of the Cell
Vol. 21, 50–62, January 1, 2010

Analyzing the Effects of Delaying Aster Separation on Furrow Formation during Cytokinesis in the *Caenorhabditis elegans* Embryo

Lindsay Lewellyn,* Julien Dumont, Arshad Desai,* and Karen Oegema*

Department of Cellular and Molecular Medicine, Ludwig Institute for Cancer Research, University of California, San Diego, La Jolla, CA 92093

Submitted January 29, 2009; Revised October 14, 2009; Accepted October 22, 2009
Monitoring Editor: Yu-Li Wang

Signaling by the centrosomal asters and spindle midzone coordinately directs formation of the cytokinetic furrow. Here, we explore the contribution of the asters by analyzing the consequences of altering interaster distance during the first cytokinesis of the *Caenorhabditis elegans* embryo. Delaying aster separation, by using TPXL-1 depletion to shorten the metaphase spindle, leads to a corresponding delay in furrow formation, but results in a single furrow that ingresses at a normal rate. Preventing aster separation, by simultaneously inhibiting TPXL-1 and Gα signaling-based cortical forces pulling on the asters, delays furrow formation and leads to the formation of multiple furrows that ingress toward the midzone. Disrupting midzone-based signaling, by depleting conserved midzone complexes, results in a converse phenotype: neither the timing nor the number of furrows is affected, but the rate of furrow ingression is decreased threefold. Simultaneously delaying aster separation and disrupting midzone-based signaling leads to complete failure of furrow formation. Based on these results, we propose that signaling by the separated asters executes two critical functions: 1) it couples furrow formation to anaphase onset by concentrating contractile ring proteins on the equatorial cortex in a midzone-independent manner and 2) it subsequently refines spindle midzone-based signaling to restrict furrowing to a single site.

INTRODUCTION

The cytokinetic furrow assembles in response to signals from the anaphase spindle, thereby coupling cytokinesis spatially and temporally to chromosome segregation (Glotzer, 2004; Eggert *et al*., 2006). Furrow formation is directed by signals from the centrosomal asters and spindle midzone (Oegema and Mitchison, 1997; Maddox and Oegema, 2003; Glotzer, 2005; Eggert *et al*., 2006); however, the nature of these signals and how they coordinately specify the formation of a single furrow at a unique site remains an important current challenge. An influential experiment addressing the relative roles of aster and midzone-based signaling was recently performed in the *Caenorhabditis elegans* embryo (Bringmann and Hyman, 2005). In this experiment, the connection between the aster and chromosomes on one side of the spindle was severed with a UV microbeam immediately after anaphase onset. Cortical forces pulling on astral microtubules moved the liberated aster away from the midzone with the attached aster, spatially separating the plane bisecting the asters from the center of the spindle midzone. In this situation, two furrows formed: an initial furrow in the plane bisecting the asters followed a few minutes later by a second furrow over the midzone. These results led to the conclusion that the asters and midzone provide sequential, redundant signals that promote furrow formation.

Recent work has suggested that dynamic astral microtubules promote furrow formation by inhibiting the accumulation of contractile ring proteins on the polar cortex, leading to their relative enrichment at the cell equator (Werner *et al*., 2007; Chen *et al*., 2008; Zhou and Wang, 2008), a role analogous to the classic polar relaxation mechanism originally proposed by Wolpert (1960) that was later refined by Borisy and White (1983). Support for this idea comes from the *C. elegans* embryo, in which misregulation of the microtubule-severing protein katanin destabilizes microtubules and leads to formation of a small spindle in the embryo posterior and accumulation of excess myosin on the opposite anterior cortex (Werner *et al*., 2007). Similarly, in grasshopper spermatocytes, asymmetrically positioned asters or placement of a mechanically "deconstructed" spindle on one side of the cell results in the accumulation of cortical actin on the opposite side of the cell (Chen *et al*., 2008). An inhibitory role for the asters has also been proposed based on work in vertebrate cells and in sea urchin embryos. In contrast to the progressive recruitment of myosin observed on the equatorial cortex in vertebrate cells, on the cortex above the asters phases of myosin recruitment were balanced by phases of loss preventing net myosin accumulation (Zhou and Wang, 2008). Similarly, sea urchin embryos undergoing anaphase onset in the presence of nocodazole, at levels sufficient to depolymerize astral microtubules, accumulate high levels of active myosin II over the entire cell cortex, rather than specifically at the cell equator. Treatment of sea urchin em-

This article was published online ahead of print in *MBC in Press* (http://www.molbiolcell.org/cgi/doi/10.1091/mbc.E09–01–0089) on November 4, 2009.

* Affiliated with the University of California–San Diego Biomedical Sciences graduate program.

Address correspondence to: Karen Oegema (koegema@ucsd.edu).

Abbreviations used: CPC, chromosomal passenger complex; NEBD, nuclear envelope breakdown; RNAi, RNA-mediated interference.

bryos with lower levels of nocodazole, which allowed cytokinesis to occur, led to increased levels of active myosin II over a substantially broader region of the equatorial cortex than in controls (Foe and von Dassow, 2008). This result suggests that by inhibiting the contractility of the polar cortex, dynamic astral microtubules limit the width of the equatorial contractile region.

Insight into the role of the asters in furrow formation can be obtained by analyzing the effect of varying interaster distance, thereby redistributing the spatial cues that the asters provide. In a classic set of experiments, Rappaport demonstrated that increasing interaster distance in manipulated sea urchin embryos inhibits furrowing: this inhibition can be overcome by moving the spindle closer to the cell surface (Rappaport, 1969). Early cytologists also reported that decreased interaster distance correlates with reduced furrowing activity (Teichmann, 1903; Wilson, 1928). The effect of experimentally reducing the rate of aster separation after anaphase onset has been investigated in the *C. elegans* embryo by inhibiting Gα signaling, which normally generates cortical forces that pull on the asters after anaphase onset to promote spindle elongation (Gönczy and Rose, 2005). Disrupting Gα signaling does not result in a cytokinesis defect on its own. However, when combined with inhibition of the spindle midzone-localized signaling complexes centralspindlin or the chromosomal passenger complex (CPC), disrupting Gα signaling leads to a synthetic defect in furrow formation (Dechant and Glotzer, 2003; Verbrugghe and White, 2007). Whether this synthetic defect is a consequence of reducing interaster distance (Dechant and Glotzer, 2003) or reflects a direct role for the Gα pathway in mediating aster-based signaling has remained controversial (Bringmann *et al*., 2007; Verbrugghe and White, 2007). Thus, the effect of reducing interaster distance on furrow formation has remained an important open question.

Here, we develop a controlled system to analyze the effects of reducing interaster distance on the cortical accumulation of contractile ring proteins and furrow formation during the first cytokinesis of the *C. elegans* embryo. We accomplish this by using TPXL-1 depletion to shorten the metaphase spindle, thereby introducing a delay between anaphase onset and the time when aster separation is comparable with that at anaphase onset in controls (Özlü *et al*., 2005). Because kinetochore microtubules exert forces that counter astral pulling forces, simultaneous inhibition of kinetochore assembly restores aster separation in TPXL-1–depleted embryos. This provides a control situation ensuring that effects on cytokinesis are specifically due to reduced interaster distance and eliminating the possibility of a direct role for TPXL-1. Our results suggest that signaling by the separated asters controls furrow formation in a midzone-independent manner by focusing global cortical contractility triggered by anaphase onset to the cell equator. Subsequently, aster-based signaling also confines the midzone-based signal to restrict furrow formation to a unique site.

MATERIALS AND METHODS

Strains and Live Imaging

The genotypes of all strains used are listed in Supplemental Table 1. The strains OD58 (Audhya *et al*., 2005), OD38, and OD73 (Maddox *et al*., 2007) were described previously. The strain JJ1473 expressing NMY-2:green fluorescent protein (GFP) (Nance *et al*., 2003) was a gift of Edwin Munro (University of Chicago). Strains were maintained at 20° and live imaging was performed on newly fertilized embryos mounted as described previously (Oegema *et al*., 2001). For most experiments, embryos were filmed using a spinning disk confocal mounted on a TE2000-E inverted microscope (Nikon , Tokyo, Japan) equipped with a krypton-argon 2.5-W water-cooled laser (Spectra Physics, San Jose, CA) and a charge-coupled device camera (Orca-ER; Hamamatsu, Hamamatsu, Japan). Acquisition parameters, shutters, and focus were controlled by MetaMorph software (Molecular Devices, Sunnyvale, CA). In all cases a 60×, 1.4 numerical aperture (NA) PlanApochromat lens with 2 × 2 binning was used. For cortical imaging, four z-sections were collected at 1-μm intervals at each time point. Furrow diameters were measured in end-on projections generated from 11- × 2.5-μm z-stacks collected at 20-s intervals. The region of the furrow was isolated, projected, and rotated 90° using MetaMorph software to generate an end-on view. Embryos coexpressing GFP:AuroraB$^{AIR\text{-}2}$ and RFP^{mCherry}:Histone H2B (OD224) were imaged on an Andor Revolution spinning disk confocal system controlled by the Andor iQ software (Andor Technology, Belfast, Ireland) equipped with an electron multiplication back-thinned charge-coupled device camera (iXon; Andor Technology) and solid state 100-mW lasers. Embryos were imaged with a 60×, 1.4 NA PlanApochromat lens with a 1.5× optivar and no binning.

Quantification of Cortical Contractile Protein Accumulation

Analysis of the postanaphase accumulation of cortical GFP:Anillin and NMY-2:GFP as a function of embryo length was performed on maximal-intensity projections of four-plane z-series containing the embryo cortex. A line bisecting the embryo was drawn from the anterior to posterior tips of the embryo, and MetaMorph software was used to generate an average intensity linescan (50 pixels wide, ~1/2 of the width of the embryo) for each time point. Embryos were divided into 20 equal length segments from anterior (0% embryo length) to posterior (100% embryo length), and the mean GFP:Anillin/NMY-2:GFP in each segment, after subtraction of a background measurement for that segment made just before anaphase onset (120–160 s after nuclear envelope breakdown [NEBD]; before detectable accumulation), was calculated for each time point. The values for each data set were normalized by dividing all intensity values by the average maximal value for controls (55–65% embryo width at 280 s after NEBD) imaged in parallel.

Analysis of GFP:AuroraB$^{AIR\text{-}2}$

The graph in Figure 4B was generated by drawing a 40-pixel wide box along the spindle axis in images of control and *tpxl-1(RNAi)* embryos acquired 120 s after anaphase onset and generating a linescan of average fluorescence intensity versus position along the spindle axis. After subtracting the cytoplasmic background (average of the final 5 values of the linescan, nearest the embryo posterior) from all values, the traces from five to six individual embryos were aligned by setting the fluorescence intensity maximum for each scan to position = 0. After aligning, the average fluorescence intensity at each position along the spindle axis was calculated for the set of scans and plotted.

RNA-mediated Interference

Double-stranded RNAs (dsRNAs) were prepared as described previously (Oegema *et al*., 2001), by using the primers listed in Supplemental Table 2 to amplify regions from N2 genomic or specific cDNAs. L4 hermaphrodites were injected with dsRNA and incubated at 20°C for 45–48 h. For double depletions, RNAs were mixed to obtain equal concentrations for each RNA. For single depletions done in parallel with double depletions, the dsRNA corresponding to the target was mixed with an equal concentration of a control RNA made by amplifying a region of the yeast gene *CTF13* that does not have significant homology with any *C. elegans* gene.

Immunofluorescence

Immunofluorescence was performed as described previously (Oegema *et al*., 2001; Desai *et al*., 2003) by using a 20-min methanol fixation. Antibodies against the C-terminal 108 amino acids of ZEN-4 were generated by using the primers (cgcgaattccaacagggttacgttaatccaaaat and cgcttccgtcgacttactttcgtgtgctcggagat) to amplify the corresponding region from a gene-specific cDNA. The fragment was digested with EcoRI/SalI and cloned into pGEX6P-1 (GE Healthcare, Little Chalfont, Buckinghamshire, United Kingdom) digested with the same enzymes. A purified glutathione transferase (GST) fusion was injected into a rabbit. Affinity purification was performed using standard procedures after coupling a fragment generated by removal of the GST by cleavage with PreScission protease (GE Healthcare) to a 1 ml of NHS HiTrap column (GE Healthcare). Affinity-purified polyclonal antibodies against the C-terminal peptide of AIR-2 (C)RAEKQQKIEKEASLRNH were generated as described previously (Desai *et al*., 2003). Immunofluorescence was performed with fluorescein isothiocyanate-labeled α-tubulin antibodies (DM1-α; Abcam, Cambridge, MA) and antibodies to ZEN-4 and AIR-2 directly labeled with cyanine (Cy)3 or Cy5 as described previously (Francis-Lang *et al*., 1999). Images were acquired using a 100×, 1.35 NA U-Planapo oil objective lens (Olympus, Tokyo, Japan) mounted on a DeltaVision system (Applied Precision, Issaquah, WA) that included an IX70 microscope (Olympus) equipped with a CoolSNAP charge-coupled device camera (Roper Scientific, Trenton, NJ). All fixed images are projections of three-dimensional (3D) widefield data sets that were computationally deconvolved using softWoRx software (Applied Precision).

Western Blotting

Western blotting of control, *tpxl-1(RNAi)*, and *tpxl-1 & hcp-4(RNAi)* worms was performed as described previously (Hannak *et al*., 2001). Western blots were initially probed using 1 μg/ml rabbit anti–TPXL-1 (Özlü *et al*., 2005), which was detected using a horseradish peroxidase-conjugated secondary antibody (1:10,000; Bio-Rad Laboratories, Hercules, CA). The same blot was subsequently probed for α-tubulin using the monoclonal DM1α (1:100; Sigma-Aldrich, St. Louis, MO) followed by an alkaline phosphatase-conjugated anti-mouse secondary antibody (1:3750; Jackson ImmunoResearch Laboratories, West Grove, PA).

RESULTS

A Controlled System to Analyze the Effects of Delaying Aster Separation on Cytokinesis

We developed a controlled system to manipulate anaphase aster separation based on depletion of the spindle protein TPXL-1, the *C. elegans* orthologue of TPX2 (Özlü *et al*., 2005). TPXL-1 depletion is an extensively characterized perturbation that has only one known phenotype—reducing spindle length by reducing the length of the kinetochore microtubules that connect the chromosomes to the spindle poles (Özlü *et al*., 2005, Srayko *et al*., 2005, Portier *et al*., 2007). TPXL-1 is an activator of Aurora A (Özlü *et al*., 2005), a mitotic kinase that has multiple functions in the early *C. elegans* embryo (Schumacher *et al*., 1998, Hannak *et al*., 2001, Portier *et al*., 2007). However, of these functions only spindle length control is mediated by TPXL-1. Depletion of TPXL-1 does not affect cell polarity, the kinetics or amount of γ-tubulin recruited to centrosomes, or the rates of centrosomal microtubule nucleation or microtubule growth (Özlü *et al*., 2005; Srayko *et al*., 2005). In addition, the asters in control and TPXL-1–depleted embryos move at a similar velocity

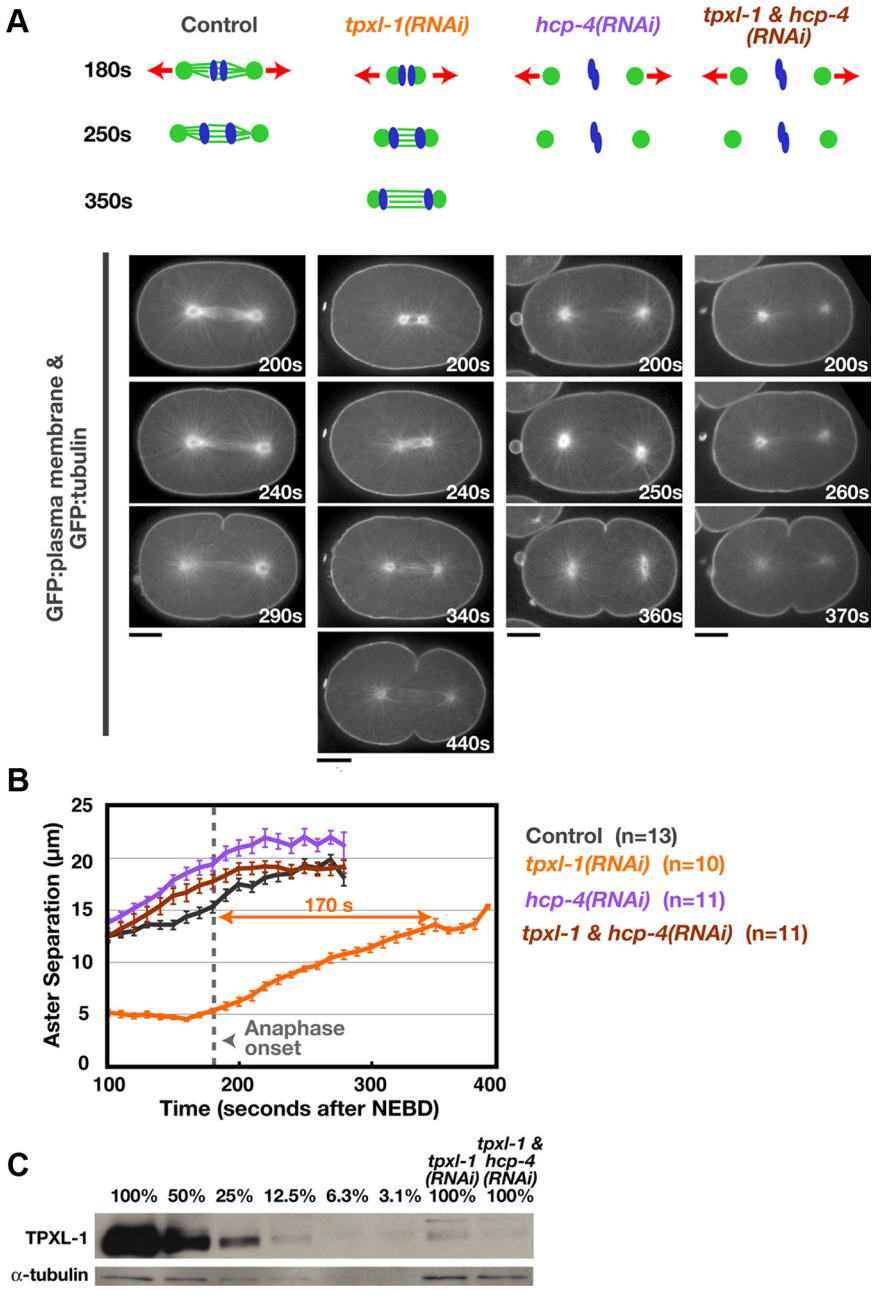

Figure 1. TPXL-1 depletion introduces a delay between anaphase onset and the point when the asters achieve a normal extent of separation. (A) Schematics summarize the effects of each perturbation. Kinetochore microtubules, which resist cortical forces that pull on astral microtubules (red arrows), are absent in *hcp-4(RNAi)* embryos. Confocal images of embryos coexpressing GFP:β-tubulin and a GFP plasma membrane probe. Times are in seconds after NEBD. Bars, 10 μm. (B) Mean aster-to-aster distance, measured from the sequences in A, is plotted versus time in seconds after NEBD. Error bars are the SEM. Dotted line marks the mean time of anaphase onset in control and TPXL-1–depleted embryos. (C) Western blot of control, *tpxl-1(RNAi)*, and *tpxl-1 & hcp-4(RNAi)* worms. Serial dilutions of the control lysate were used to quantify the amount of TPXL-1 in the RNAi samples (percentage of amount in 100% control indicated above each lane). RNAi of *tpxl-1* alone and *tpxl-1 & hcp-4* reduced TPXL-1 levels to 7.4 and 5.6% of that in controls, respectively.

and reach a similar final position after spindle severing by using a UV laser (Özlü *et al.*, 2005), which in light of recent modeling (Kozlowski *et al.*, 2007) suggests that TPXL-1 depletion does not substantially alter either the number of astral microtubules or the Gα signaling-mediated forces that position the asters. Nevertheless, it was important to control for the possibility that TPXL-1 has a direct, unidentified role in cytokinesis. To do this, we used codepletion of the inner kinetochore component HCP-4 (the *C. elegans* CENP-C orthologue), which rescues the spindle shortening phenotype of TPXL-1 depletion by disrupting the kinetochore microtubules that connect the chromosomes to the spindle poles (Oegema *et al.*, 2001; Özlü *et al.*, 2005).

TPXL-1 depletion reduces the length of the metaphase spindle from ~15 to 5 μm (Figure 1, A and B; Özlü *et al.*, 2005). The short spindles remain centered within the embryo so that the spindle center is the same distance from the equatorial cortex as in control embryos (Supplemental Figure S1). Anaphase onset also occurs with the same timing in control and TPXL-1–depleted embryos, ~180 s after nuclear envelope breakdown (180 ± 14.7 s [SD] in *tpxl-1(RNAi)*, n = 13; 173 ± 11.2 s [SD] in control, n = 9). After anaphase onset, the interaster distance in TPXL-1–depleted embryos increases at a linear rate for ~170 s, after which it plateaus at a value comparable with that at anaphase onset in control embryos (Figure 1, A and B). Thus, TPXL-1 depletion introduces an ~3-min delay between anaphase onset and the point when the asters achieve a normal extent of separation, allowing us to assess the effect of this delay on furrow formation.

HCP-4 depletion leads to premature aster separation due to the absence of kinetochore microtubules, which normally resist the outward-directed cortical pulling forces acting on the asters (Oegema *et al.*, 2001). Embryos depleted of HCP-4 or codepleted of TPXL-1 and HCP-4 exhibit a similar pattern of premature aster separation (Figure 1, A and B, and Supplemental Movie S1). Quantitative immuno-blotting confirmed that TPXL-1 levels were reduced to a similar extent when depleted on its own or in conjunction with HCP-4 (Figure 1C). Thus, the ability to rescue aster separation in TPXL-1–depleted embryos via codepletion of HCP-4 provides a controlled system to characterize the consequences of delaying aster separation on cytokinesis.

Delaying Aster Separation Leads to a Corresponding Delay in Furrow Formation but Does Not Alter the Ingression Rate

To examine the effect of delaying aster separation on cytokinesis, we analyzed embryos expressing a GFP-labeled plasma membrane probe (Audhya *et al.*, 2005). To score furrow formation unambiguously, we measured the time between NEBD and "furrow involution"—the first appearance of a furrow composed of two adhered back-to-back plasma membranes in a side view of the embryo (purple arrowheads in Figure 2A). Relative to controls, furrow involution was delayed by ~190 s in TPXL-1–depleted embryos (Figure 2, A and B, and Supplemental Movie S2). To measure the kinetics of furrow ingression, z-stacks were collected and the region containing the furrow was rotated by 90° and projected to generate an end-on view of the division plane (Figure 2C). The diameter of the circular hole between the daughter cells was measured at each time point. This analysis revealed that after furrow formation in TPXL-1–depleted embryos, the rate of furrow ingression and the

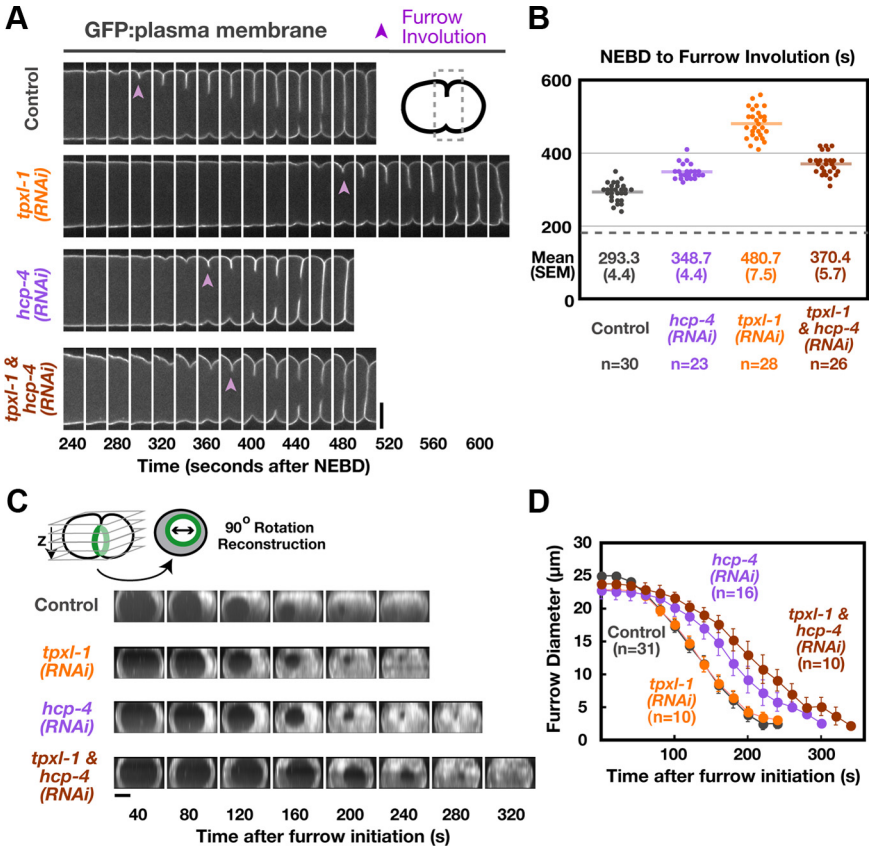

Figure 2. Delaying aster separation leads to a corresponding delay in furrow formation but does not alter the ingression rate. (A) Montages of the equatorial region from central plane images of embryos expressing a GFP plasma membrane probe. Furrow involution is indicated (purple arrowheads). (B) The interval between NEBD and furrow involution, measured in embryos coexpressing GFP:β-tubulin and a GFP plasma membrane probe, is plotted for individual embryos. Solid line indicates the mean. Dashed line indicates the mean time of anaphase onset in controls. (C) Spinning disk confocal optics were used to image control, *tpxl-1(RNAi)*, *hcp-4(RNAi)*, and *tpxl-1 & hcp-4(RNAi)* embryos expressing the GFP plasma membrane probe. For each time point, 11 images were collected at 2.5-μm intervals in z and an "end-on" view of the division plane was obtained by isolating the region of the furrow from the image stack, rotating it by 90° and generating a maximum intensity projection. Representative projections from time-lapse series are shown for each condition. (D) Mean furrow diameter was measured from end on reconstructions generated as described in C and is plotted versus time. Times in C and D are in seconds after furrow initiation, the time when the first detectable ingression was visible. Error bars are SEM. Bars, 10 μm.

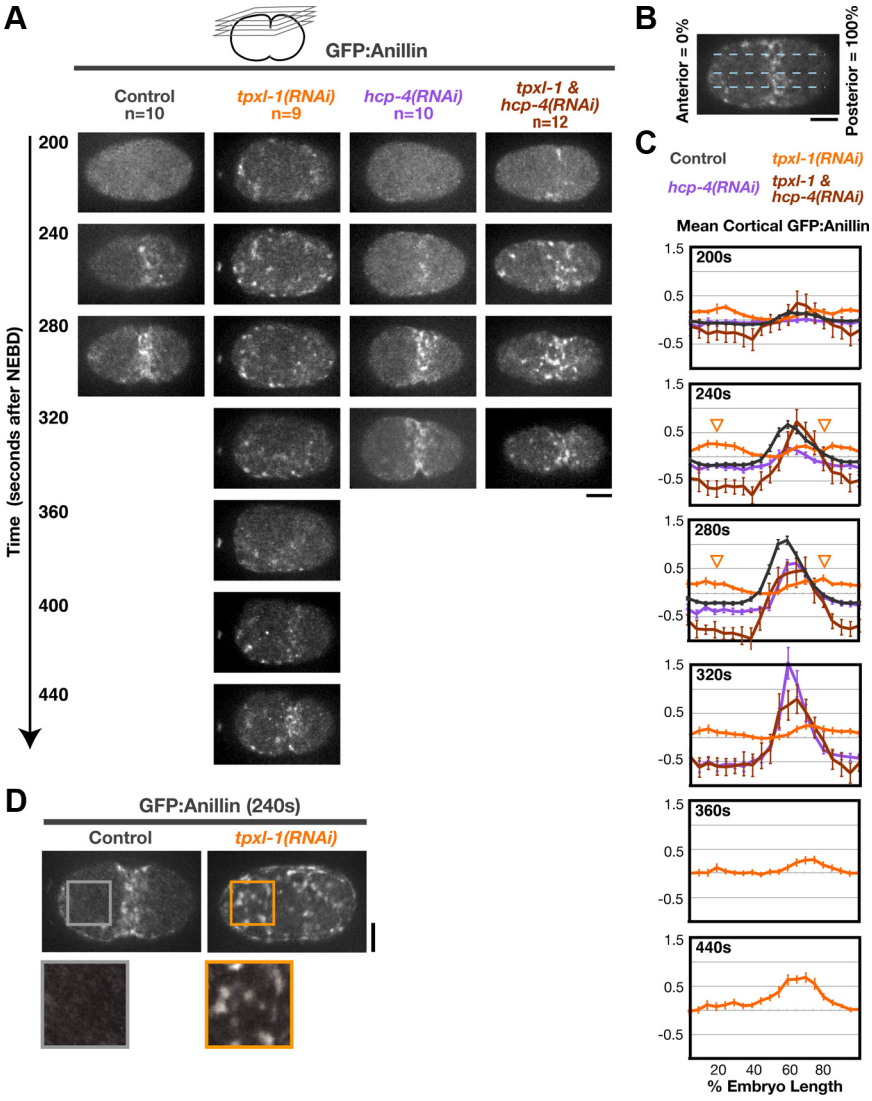

Figure 3. Aster separation is required for the equatorial enrichment of contractile ring proteins following anaphase onset. (A) Images of the cortex in embryos expressing GFP:Anillin. Images are maximum intensity projections of four z-sections collected at 1-μm intervals (see schematic). (B) Schematic illustrating the method used to analyze cortical GFP:Anillin distribution. A 50-pixel-wide line (~1/2 the embryo width) was drawn, and embryos were divided into 20 equal length segments from anterior (0%) to posterior (100%). (C) The mean postanaphase accumulation of cortical GFP:Anillin is plotted as a function of embryo length. The mean GFP:Anillin in each segment, after subtraction of a background measurement made before anaphase onset, is plotted for each time point. Values were normalized by dividing by the average maximum value for controls. In TPXL-1–depleted embryos, a slight enrichment of cortical GFP:Anillin is observed on the polar cortices (arrowheads in graphs for 240- and 280-s time points) relative to the equator. Error bars are SEM (D) Examples of cortical GFP:Anillin accumulation in control and *tpxl-1(RNAi)* embryos 240 s after NEBD. Boxed regions are magnified 2×. Times are in seconds after NEBD. Bars, 10 μm.

ultimate success of cytokinesis were indistinguishable from controls (Figure 2D; compare the orange and gray curves).

To ensure that the delay in furrow formation was not due to a direct role for TPXL-1 in cytokinesis, we next examined embryos codepleted of TPXL-1 and HCP-4. Depletion of HCP-4 on its own led to a modest delay of ~55 s in furrow involution and a slight decrease in the ingression rate (Figure 2, A–D). This phenotype is common to perturbations that disrupt kinetochore function (data not shown) and probably results from the consequences of disrupting chromosome segregation on assembly of the spindle midzone. Codepletion of HCP-4 and TPXL-1 rescued the 190-s delay in furrow involution resulting from TPXL-1 depletion back to the modest delay seen in embryos depleted of HCP-4 alone (Figure 2, A and B). Thus, the delay in furrow formation in TPXL-1–depleted embryos is a consequence of delaying aster separation and does not reflect an independent role for TPXL-1 in promoting cytokinesis. The fact that delaying aster separation leads to a matched delay in furrow formation indicates that separated asters are required to temporally couple furrow formation to anaphase onset.

Aster Separation Is Required for the Equatorial Enrichment of Contractile Ring Proteins after Anaphase Onset

To understand how delaying aster separation delays furrow formation, we next examined the consequences of delaying aster separation on the cortical accumulation of GFP fusions with two contractile ring components, Anillin (GFP:Anillin$^{ANI\text{-}1}$; Figure 3 and Supplemental Movie S3) and the heavy chain of myosin II (NMY-2:GFP; Supplemental Figure S2). The postanaphase pattern of equatorial accumulation was essentially identical for the two markers (Figure 3, A–C, and Supplemental Figure S2, A and B). In control embryos, GFP:Anillin and NMY-2:GFP accumulated on the equatorial cortex during the 100 s after anaphase onset (180–280 s after NEBD), forming a band that peaked at ~60% of embryo length. Furrow involution occurred ~10 s after the equatorial band reached its maximal intensity (Figure 3C; 280 s). In TPXL-1–depleted embryos, GFP:Anillin and NMY-2:GFP also accumulated on the cortex during the 100 s after anaphase onset. However, instead of being concentrated at the cell equator, patches of GFP:Anillin and NMY-2:GFP were distributed over the entire cortex (Figure 3, A and D; Supplemental Figure S2, A and C; and Supplemental Movie S3).

Quantitative analysis revealed a slight enrichment of cortical GFP:Anillin on the anterior and posterior cortices relative to the cell equator (Figure 3C, arrowheads in graphs for 240- and 280s time points)—a pattern inverse to that seen in controls at this time. Thus, separated asters are critical for the equatorial enrichment of contractile ring proteins after anaphase onset.

After an ~3-min delay, the interaster distance in TPXL-1–depleted embryos is similar to that at anaphase onset in control embryos. At this point, an equatorial band of GFP:Anillin and NMY-2:GFP has formed on the cortex, reaching ~50% of the levels in controls (Figure 3C; 440 s). The 3-min delay in the equatorial accumulation of GFP:Anillin and NMY-2:GFP (Figure 3, A and C, and Supplemental Figure S2, A and B) paralleled the ~3-min delay in furrow involution (Figure 2, A and B). Codepletion of HCP-4 along with TPXL-1 rescued the delay in the equatorial accumulation of GFP:Anillin and NMY-2:GFP to yield a pattern similar to that in controls (Figure 3, A and C; Supplemental Figure S2, A and B; and Supplemental Movie S3). We note that although GFP:Anillin and NMY-2:GFP accumulated with normal timing, the equatorial accumulation persisted for ~40 s longer in embryos depleted of HCP-4 alone or HCP-4 and TPXL-1 (Figure 3, A and C), due to the delay in furrow involution resulting from HCP-4 depletion (Figure 2, A and B). Together, these results show that the delays in the equatorial accumulation of contractile ring proteins and furrow formation in TPXL-1–depleted embryos are due to the delay

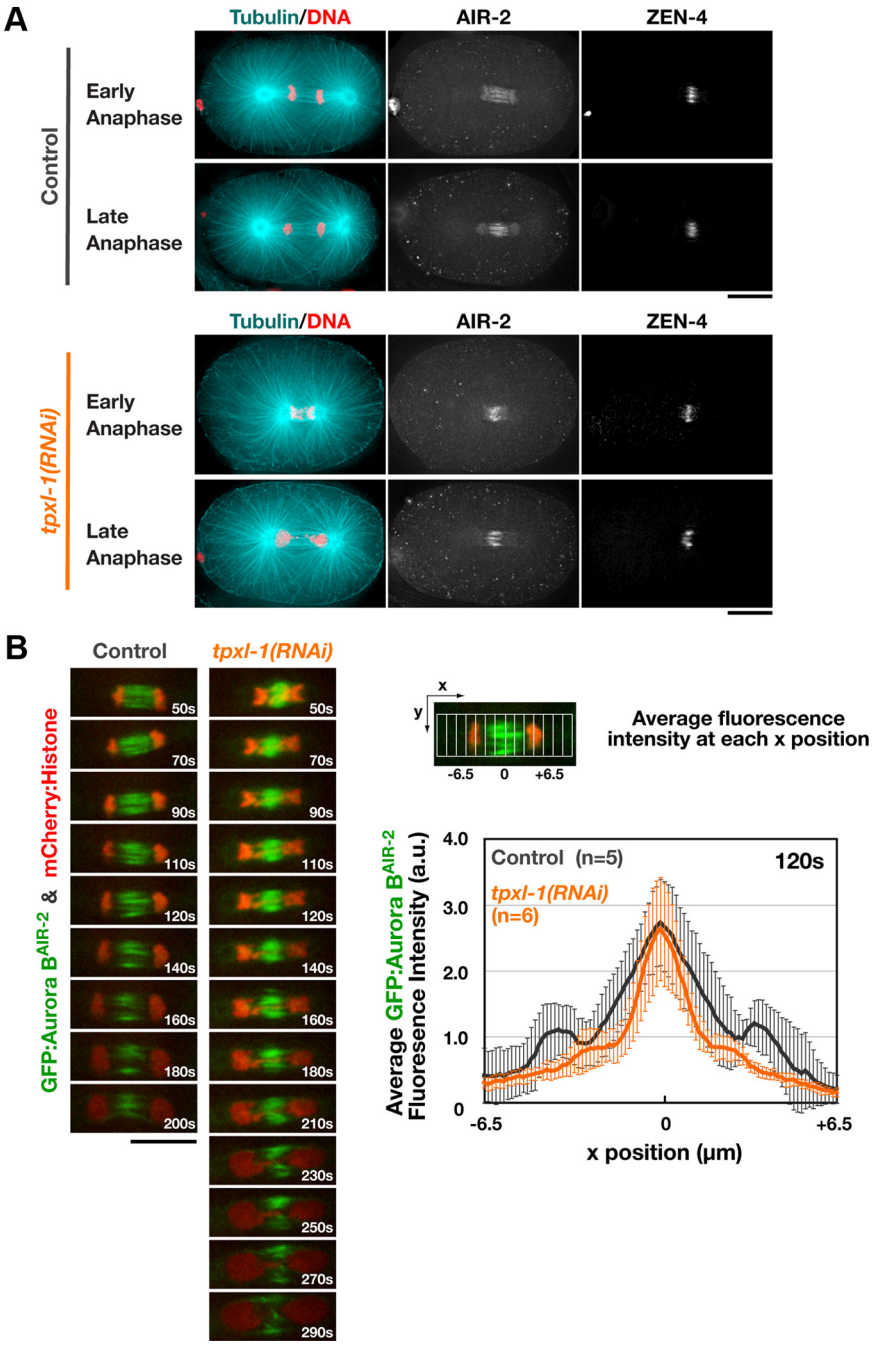

Figure 4. TPXL-1 depletion does not significantly alter the localization of midzone-localized signaling complexes. (A) Fixed control and *tpxl-1(RNAi)* embryos were stained to visualize DNA, α-tubulin, ZEN-4, and AIR-2. 3D widefield data stacks were collected and computationally deconvolved. Maximum intensity projections of the central region of representative early (top) and late (bottom) anaphase embryos are shown. (B) Single-plane confocal images of the spindle in embryos expressing GFP:AuroraB^{AIR-2} and mCherry:Histone H2B. Times are relative to anaphase onset. Graph shows the average GFP:AuroraB^{AIR-2} fluorescence intensity as a function of position along the spindle axis (see diagram) in control and *tpxl-1(RNAi)* embryos 120 s after anaphase onset, which corresponds to the time of furrow involution in controls. Values are plotted over the length of the midzone, with the zero position corresponding to the fluorescence intensity maximum. Error bars are the SD. Bars, 10 μm.

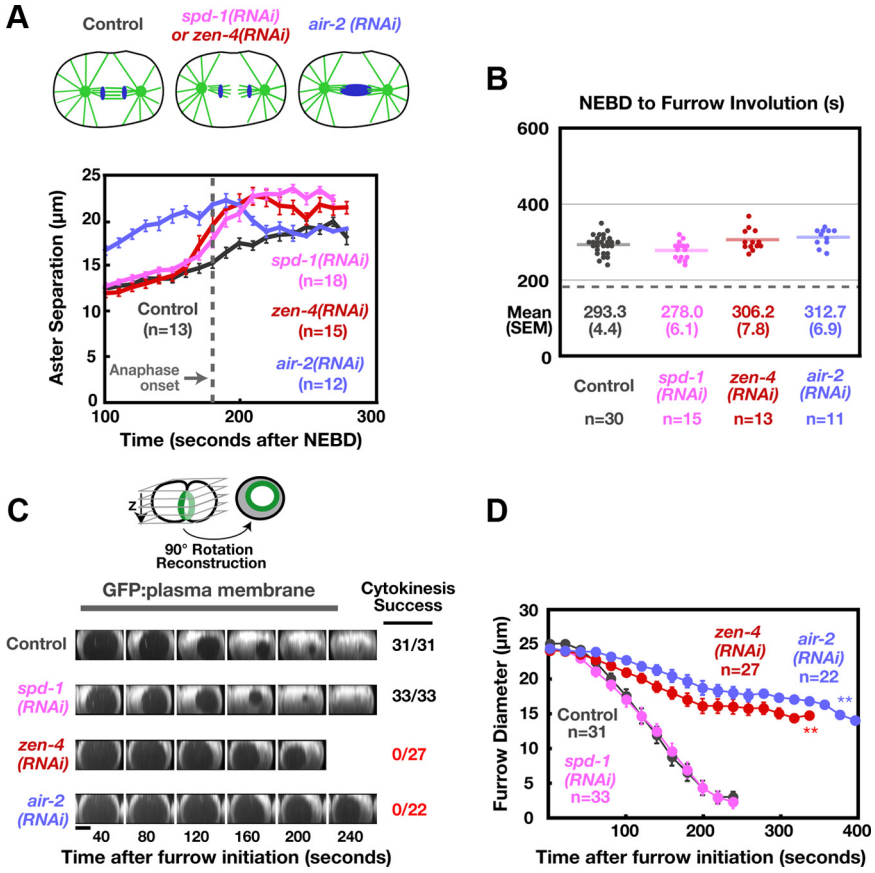

Figure 5. Furrows form with normal timing but ingress at a reduced rate after inhibition of centralspindlin or the chromosomal passenger complex. (A) Schematics summarize the effects of each perturbation on chromosome segregation and anaphase spindle structure. The mean aster-to-aster distance, measured from confocal images of embryos coexpressing GFP:β-tubulin and a GFP plasma membrane probe, is plotted versus time in seconds after NEBD for each condition. The control curve from Figure 1B is reproduced for comparison. Dotted line indicates anaphase onset in controls. Error bars are SEM. (B) The interval between NEBD and furrow involution, measured in embryos coexpressing GFP:β-tubulin and a GFP plasma membrane probe, is plotted for individual embryos. The data for the control embryos is reproduced from Figure 2B for comparison. Solid line indicates the mean. Dashed line indicates the mean time of anaphase onset in controls. (C) Spinning disk confocal optics were used to acquire z-series of control, *spd-1(RNAi)*, *zen-4(RNAi)*, and *air-2(RNAi)* embryos expressing the GFP plasma membrane probe, and reconstructions yielding an "end-on" view of the division plane were generated. Representative projections from time-lapse series are shown for each condition. The fraction of embryos that completed the first cytokinesis is indicated to the right. Bar, 10 μm. (D) Mean furrow diameter was measured from end on reconstructions generated as in C and is plotted versus time. The control curve is reproduced from Figure 2D for comparison. Times in C and D are in seconds after furrow initiation, the time when the first detectable ingression was visible. Error bars are the 90% confidence interval for the mean. Double asterisks indicate furrow regression.

in aster separation and not to a specific role for TPXL-1 in cytokinesis.

TPXL-1 Depletion Does Not Significantly Alter the Localization of Midzone-localized Signaling Complexes

TPXL-1 depletion leads to matched delays in aster separation, the equatorial recruitment of contractile ring proteins, and furrow formation. These delays are rescued when aster separation is restored by codepletion of the kinetochore protein HCP-4, suggesting that they are a consequence of the effect of TPXL-1 on the kinetics of aster separation, rather than an unintended consequence of TPXL-1 depletion on assembly of the spindle midzone. To confirm this conclusion, we analyzed the effect of TPXL-1 depletion on the localization of centralspindlin and the CPC, two midzone-localized complexes required for cytokinesis (Powers *et al*., 1998; Raich *et al*., 1998; Schumacher *et al*., 1998; Jantsch-Plunger *et al*., 2000; Kaitna *et al*., 2000; Severson *et al*., 2000). Immunofluorescence revealed that TPXL-1–depleted embryos exhibit mild defects in chromosome segregation due to the dramatically shortened spindle (Figure 4A). However, the localization of AuroraB^{AIR-2} kinase, the essential enzymatic component of the CPC, and the centralspindlin component ZEN-4, seemed similar between control and *tpxl-1(RNAi)* embryos (Figure 4A). Live imaging of embryos coexpressing GFP:AuroraB^{AIR-2} and mCherry:Histone H2B confirmed the presence of a robust midzone (Figure 4B and Supplemental Movie S4). Comparison of the GFP:AuroraB^{AIR-2} fluorescence intensity along the spindle axis 120 s after anaphase onset, which corresponds to the time of furrow formation in controls, revealed that peak GFP:AuroraB^{AIR-2} levels were similar in *tpxl-1(RNAi)* embryos compared with controls; however, the distribution was slightly narrower (Figure 4B). We conclude that midzone structure is largely normal in TPXL-1–depleted embryos.

Furrows Form with Normal Timing but Ingress at a Reduced Rate after Inhibition of Centralspindlin or the Chromosomal Passenger Complex

To understand the relative contributions of signaling by the asters and midzone during cytokinesis, we tested whether inhibition of midzone-localized proteins would result in a delay in furrow formation comparable with that resulting from delaying aster separation. Using the methods we developed to characterize TPXL-1–depleted embryos, we analyzed the phenotype of embryos depleted of three different midzone proteins—the centralspindlin component ZEN-4, the CPC component AuroraB^{AIR-2}, and SPD-1, a microtubule-binding protein required for the stable bundling of midzone microtubules (Vebrugghe and White, 2004). Depletion of any of these midzone components disrupts the formation of midzone microtubule bundles and leads to premature spindle pole separation (Figure 5A). Depletion of AuroraB^{AIR-2} additionally results in defects in meiotic and mitotic chromosome segregation, which probably underlies the different aster separation kinetics for this depletion compared with depletion of SPD-1 or ZEN-4 (Figure 5A). Although midzone microtubules failed to form stable bundles

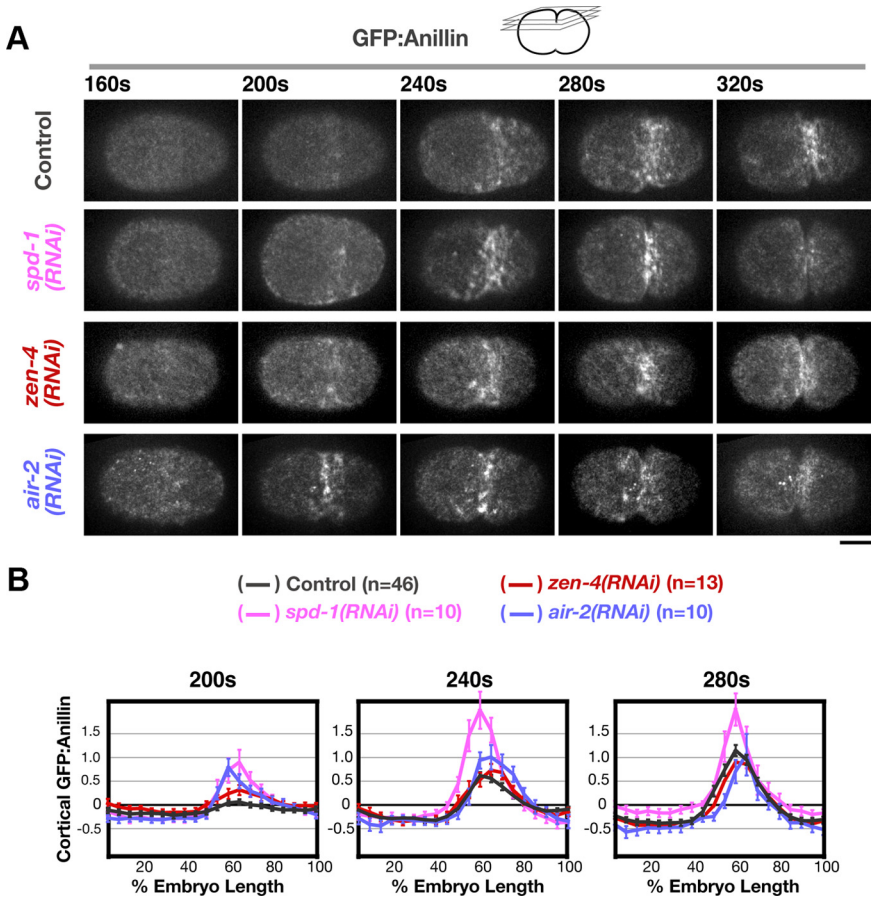

Figure 6. GFP:Anillin accumulates on the equatorial cortex with normal timing after depletion of SPD-1, ZEN-4, or AuroraB^{AIR-2}. (A) Spinning disk confocal optics were used to image the cortex in control (n = 46), *spd-1(RNAi)* (n = 10), *zen-4(RNAi)* (n = 13), and *air-2(RNAi)* (n = 10) embryos expressing GFP:Anillin. Images are maximum intensity projections of four cortical sections collected at 1-μm z intervals. (B) The mean postanaphase accumulation of cortical GFP:Anillin was quantified as a function of embryo length (as described for Figure 3) for control, *spd-1(RNAi)*, *zen-4(RNAi)*, and *air-2(RNAi)* embryos at the indicated time points after NEBD. Error bars are SEM. Bar, 10 μm.

(Supplemental Figure S3), the equatorial recruitment of contractile ring proteins and furrow formation occurred with normal timing in SPD-1–depleted embryos (Figures 5B and 6, A and B), and the rate of furrow ingression and success of the first cytokinesis were not different from controls (Figure 5, C and D). The ability of SPD-1–depleted embryos to undergo a normal division may be due to the fact that the CPC and centralspindlin continue to localize to microtubules in the midzone region, despite the failure to form stable microtubule bundles (Supplemental Figure S3).

In contrast to depletion of SPD-1, depletion of ZEN-4 or AuroraB^{AIR-2} led to penetrant failure of the first cytokinesis (Figure 5C). It is interesting to note that in ZEN-4– or AuroraB^{AIR-2}–depleted embryos, the equatorial recruitment of contractile ring proteins and furrow formation occurred with normal timing (Figures 5B and 6, A and B), but the subsequent rate of furrow ingression was dramatically (~3- to 4-fold) reduced compared with controls (Figure 5, C and D). Thus, inhibiting midzone signaling via depletion of centralspindlin or the CPC leads to a phenotype that is essentially the opposite of that resulting from delaying aster separation. Delaying aster separation delays furrow formation but does not affect the rate of furrow ingression, whereas inhibiting midzone signaling does not affect the timing of furrow formation but reduces the rate of furrow ingression. The mirror image relationship between these phenotypes suggests that the asters govern the initial patterning of cortical contractility and the timing of furrow formation, after which a hand-off is made to the spindle midzone, which controls furrow ingression.

Midzone-localized Signaling Complexes Become Essential for Furrow Formation When Aster Separation Is Delayed

The opposite phenotypes resulting from delaying aster separation and inhibiting midzone signaling suggest that simultaneous inhibition of aster separation and midzone signaling would abolish furrow formation. To test this idea, we codepleted TPXL-1 and either ZEN-4 or Aurora B^{AIR-2}. The kinetics of aster separation in the codepleted embryos were similar to those in embryos depleted of TPXL-1 alone (Figure 7, A and B); however, furrow involution was abolished (Figure 7C and Supplemental Movie S5). This suggests that when aster separation is delayed, furrow formation becomes dependent on centralspindlin and the CPC.

Multiple Furrows Form and Simultaneously Ingress toward the Spindle Center When Aster Separation Is Prevented

Although they are initially closer together, the asters in TPXL-1–depleted embryos separate after anaphase onset at the same rate as in controls, due to the action of cortical pulling forces mediated by the Gα signaling pathway (Gönczy and Rose, 2005). Thus, the asters ultimately achieve a normal extent of separation and furrowing proceeds. To determine whether the midzone can direct furrowing in the presence of unseparated asters, we examined the consequences of simultaneously depleting TPXL-1 and disrupting Gα signaling. As predicted, codepletion of TPXL-1 and GPR-1/2, essential components of the Gα signaling pathway, reduced both the interaster distance at anaphase onset and the rate of postanaphase aster separation (Figure 8, A and B).

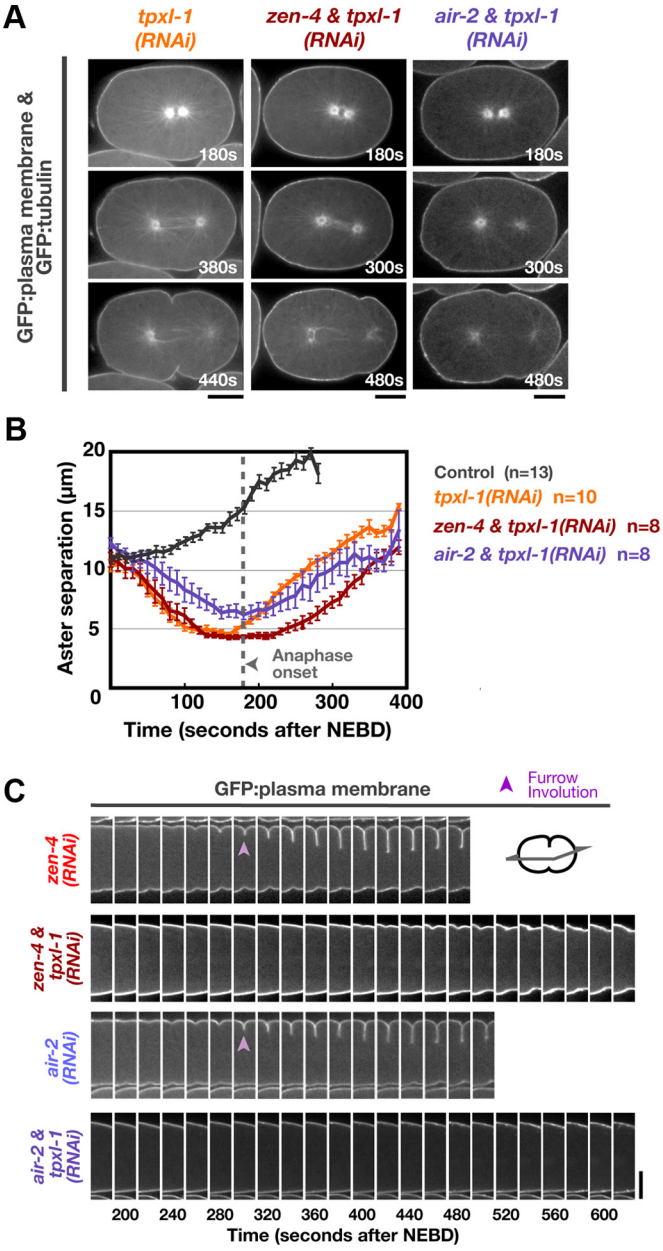

Figure 7. Midzone-localized signaling complexes become essential for furrow formation when aster separation is delayed. (A) Confocal images of *tpxl-1(RNAi)*, *zen-4 & tpxl-1(RNAi)*, and *air-2 & tpxl-1(RNAi)* embryos coexpressing GFP:β-tubulin and a GFP plasma membrane probe. (B) The mean aster-to-aster distance, measured from the sequences in A, is plotted versus time in seconds after NEBD for each condition. The control and *tpxl-1(RNAi)* curves from Figure 1B are reproduced here for comparison. Error bars are SEM. (C) Central plane confocal images of embryos expressing a GFP plasma membrane probe. Montages of the equatorial region are shown: furrow involution is indicated (purple arrowheads). The number of embryos forming a double membrane furrow is indicated. Times are in seconds after NEBD. Bars, 10 μm.

Although the asters never reached the same degree of separation as in controls, codepleted embryos formed furrows after a delay of ~4 min (Figure 8E; compared with ~3 min in embryos depleted of TPXL-1 alone). Strikingly, in ~80% of the TPXL-1– and GPR-1/2–depleted embryos, extra ingressions formed over the central third of the embryo (Figure 8, C and D). In ~50% of codepleted embryos, the multiple ingression sites matured into extra double-membrane furrows that simultaneously progressed toward the spindle center; in the other 30%, the ectopic ingression sites did not resolve into extra furrows (Figure 8, C and D, and Supplemental Movie S6). Once formed, furrows always ingressed along a trajectory toward the spindle center rather than straight into the embryo from their point of origin. Consistent with the formation of multiple furrows, the equatorial accumulation of GFP:Anillin occurred later and over a substantially broader region when aster separation was prevented by codepletion of TPXL-1 and GPR-1/2 than when aster separation was delayed by TPXL-1 depletion (Supplemental Figure S4). In 75% of embryos, the first furrows to contact the midzone from opposite sides of the embryo formed a stable connection and cytokinesis succeeded; however, in the remaining ~25% of cases, cytokinesis failed.

Cumulatively, these results suggest that when aster separation is prevented, the midzone is ultimately able to drive furrow formation. However, in the absence of support from the separated asters, the midzone-based signal is not sufficient to limit furrow formation to a single plane, and multiple furrows form and ingress toward the spindle center simultaneously.

DISCUSSION

In a classic set of experiments in flattened dispermic echinoderm eggs, Rappaport (1969) showed that increasing interaster distance by ~25% blocked furrowing over the nor-

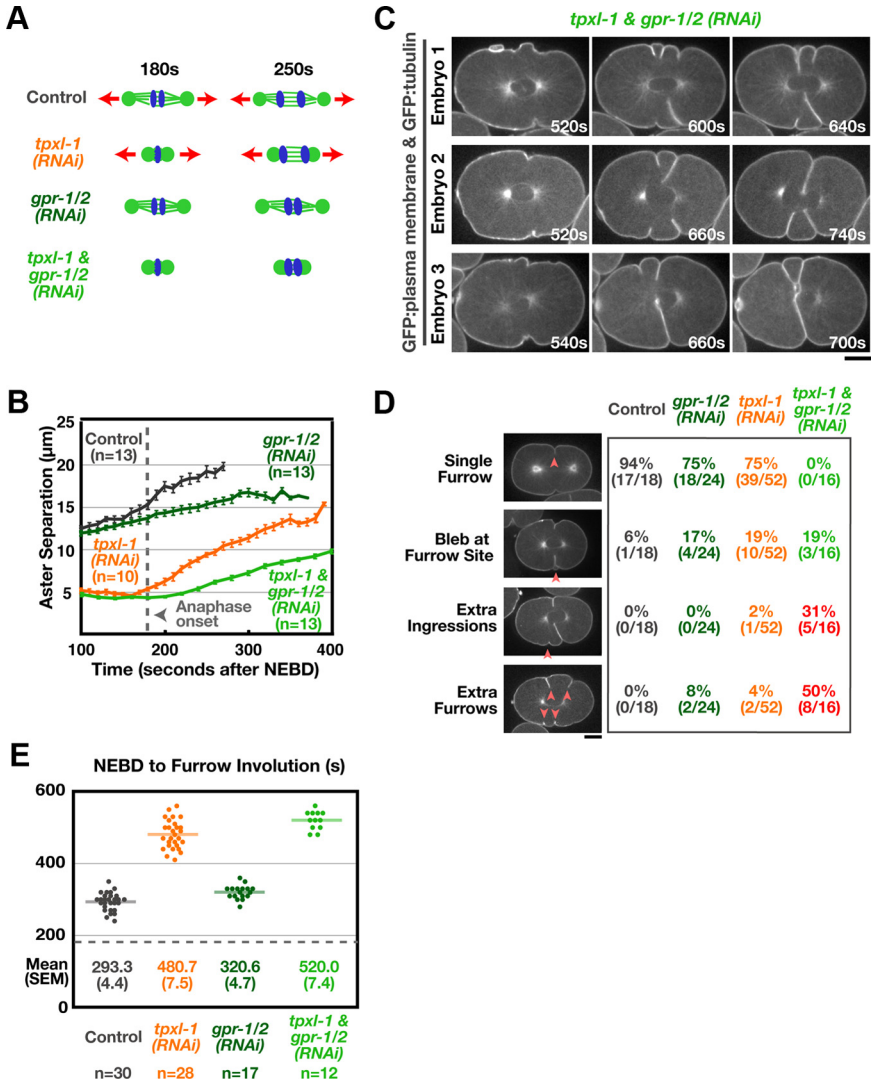

Figure 8. Multiple furrows form and simultaneously ingress toward the spindle center when aster separation is prevented. (A) Schematics illustrating the effects of each perturbation. (B) Mean aster-to-aster distance, measured in confocal images of embryos coexpressing GFP:β-tubulin and a GFP plasma membrane probe, is plotted versus time in seconds after NEBD for *gpr-1/2(RNAi)* and *tpxl-1 & gpr1/2(RNAi)* embryos. The control and *tpxl-1(RNAi)* curves from Figure 1B are reproduced here for comparison. Error bars are SEM. (C) Three examples of *tpxl-1 & gpr-1/2(RNAi)* embryos coexpressing the GFP plasma membrane probe and GFP:β-tubulin. Times are relative to NEBD. (D) Table showing the proportion of embryos exhibiting each phenotype. Red arrowheads indicate extra ingressions or furrows. (E) The interval between NEBD and furrow involution is plotted for individual embryos. The data for the control and *tpxl-1(RNAi)* embryos is reproduced from Figure 2B for comparison. Solid line indicates the mean for each condition. Dashed line indicates mean time of anaphase onset in controls.

mal range of spindle to surface distances. The ability of these overseparated asters to promote furrow formation could be rescued by moving the asters twofold closer to the cortex. Here, we perform the converse experiment, using a genetic perturbation to examine the effect of reducing interaster distance on furrow formation. TPXL-1 depletion reduces interaster distance at anaphase onset to one third of its normal value; after anaphase onset, interaster distance gradually increases over a 3-min period until it reaches a value comparable with that at anaphase onset in control embryos. Because this perturbation leads to a full 3-min delay in furrow formation, it suggests that an interaster distance comparable with that at anaphase onset in control embryos is required to form a furrow during the normal postanaphase interval. Therefore, a unifying conclusion that emerges from Rappport's experiments and our work is that furrow formation is remarkably sensitive to changes in interaster distance. We note that when aster separation is prevented rather than delayed, by simultaneous inhibition of TPXL-1 and Gα signaling-based cortical forces pulling on the asters, multiple furrows form after an extended delay. Thus, although aster separation is required to couple furrow formation to anaphase onset and to properly specify furrow position and number, furrows can ultimately form in the presence of unseparated asters.

Signaling by the Separated Asters Concentrates Contractile Ring Proteins on the Equatorial Cortex and Generates a Midzone-independent Signal for Furrow Formation

Our data show that aster separation is essential for the temporal coupling between furrow formation and anaphase onset. When aster separation was delayed, we observed an inverted pattern of contractile ring protein accumulation following anaphase onset—ectopic accumulation of contractile ring proteins on the polar cortex and a relative lack of accumulation on the equatorial cortex (Figure 3). In light of prior work indicating that microtubule asters inhibit the accumulation of contractile ring proteins (Wolpert, 1960; White and Borisy, 1983; Werner *et al*., 2007; Chen *et al*., 2008; Foe and von Dassow, 2008; Zhou and Wang, 2008), we propose a model to explain this result in which the separated asters promote furrow formation by preventing the accumulation of contractile ring proteins on the polar cortex, thereby restricting their accumulation to the cell equator (Figure 9).

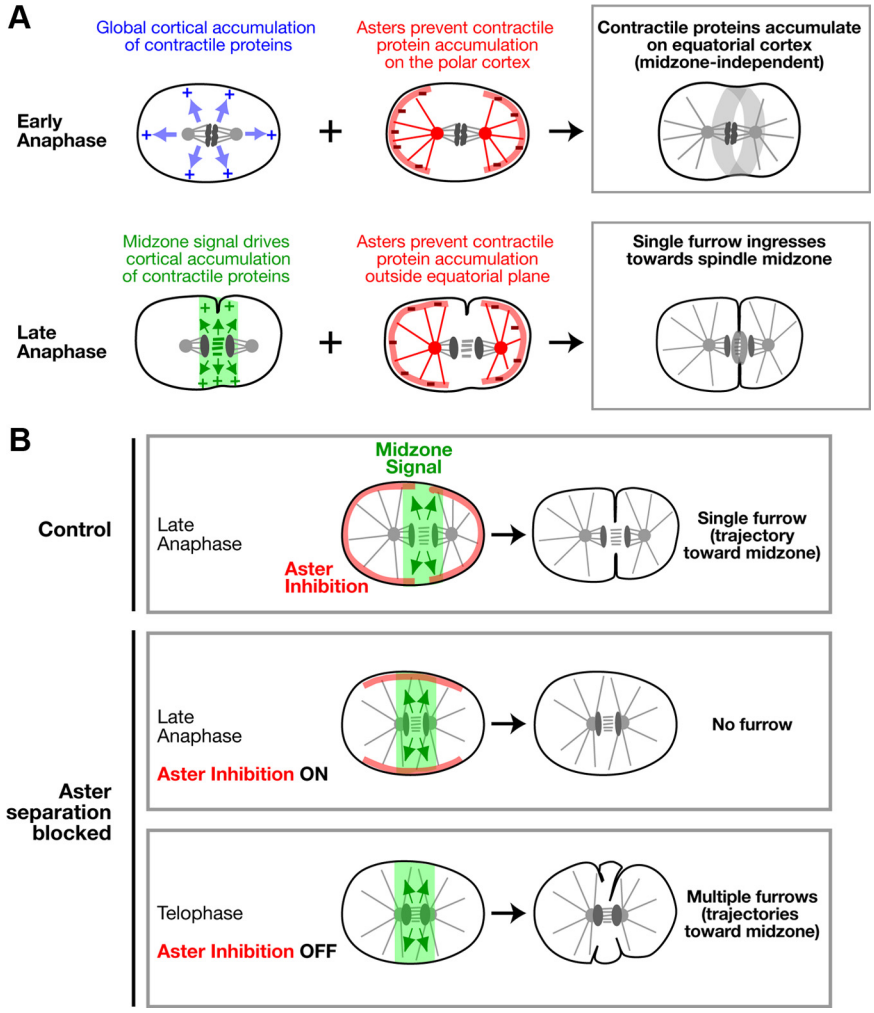

Figure 9. Signaling by the separated asters makes two distinct contributions to cytokinesis. (A) Model for the role of aster-based signaling during cytokinesis. Anaphase onset triggers a rapid global increase in cortical contractility (blue arrows; Canman *et al*., 2000; Foe *et al*., 2000; Shuster and Burgess, 2002; Straight *et al*., 2003; Foe and von Dassow, 2008). Aster-based inhibition (red lines) prevents the contractile proteins from accumulating on the polar cortex in response to this cell-cycle trigger, leading to their relative enrichment on the equatorial cortex. This mechanism provides an initial midzone-independent signal for furrow formation. As the midzone assembles, it provides a second spatially restricted signal (mediated by centralspindlin and the CPC; green arrows/zone) that promotes contractile protein accumulation. Aster-based inhibition prevents the accumulation of contractile proteins outside the equatorial plane in response to the midzone signal, confining furrow formation to a single site. (B) Model to explain the consequences of inhibiting aster separation. In control embryos at late anaphase, aster separation generates a central zone relatively devoid of aster-based inhibition. A signal generated by the spindle midzone (green arrows/zone), acts on this permissive zone to direct the formation of a single furrow that ingresses along a trajectory toward the spindle center (control; top row). When the asters fail to separate, there is no permissive zone and aster-based inhibition blocks furrow formation by preventing the accumulation of contractile proteins on the equatorial cortex—no furrow forms during the time window when cytokinesis would normally occur (aster separation blocked—late anaphase; middle row). Later, after furrowing has completed in controls, aster based inhibition decays (aster separation blocked—telophase; bottom row), and the midzone acts on the cortex to promote furrow formation in the presence of the unseparated asters. In the absence of aster-based inhibition, the midzone-based signal lacks sufficient positional information to specify a single furrow, and it promotes the simultaneous formation of multiple furrows that ingress toward the spindle center.

The spindle severing experiments of Bringmann and Hyman (2005) indicated that the asters provide an initial signal for furrow formation that is independent of a second signal from the spindle midzone. The opposite phenotypes we observed after TPXL-1 depletion versus inhibition of midzone signaling provide strong support for the idea that the asters control the initial stages of furrow formation in a midzone-independent manner. Delaying aster separation leads to an inability to properly pattern cortical contractility after anaphase onset and delays furrow formation. By contrast, inhibition of midzone signaling by depletion of essential components of either the centralspindlin or chromosomal passenger complexes does not affect the equatorial accumulation of contractile ring proteins or the timing of furrow formation. We propose that the separated asters provide a midzone-independent signal by modulating a transient, global up-regulation of contractility triggered by anaphase onset (Canman *et al*., 2000; Foe *et al*., 2000; Shuster and Burgess, 2002; Straight *et al*., 2003; Foe and von Dassow, 2008) that is independent of the midzone complexes (Figure 9A, top row). The idea that astral inhibition modulates a transient contractility wave would also explain why furrow formation requires midzone-localized signaling complexes when aster separation is delayed but not when the asters separate with normal timing (Figure 7). In TPXL-1–depleted embryos, the transient cell cycle progression driven wave of contractility is over by the time the asters separate, depriving them of their ability to generate a midzone-independent signal for furrow formation.

An inhibitory mechanism for the asters is attractive, because in addition to explaining how separated asters pattern the cortical accumulation of contractile proteins triggered by anaphase onset to promote furrow formation, it also suggests that unseparated asters would prevent the midzone-based signal from acting on the equatorial cortex. The ectopic inhibition of cortical contractility by the unseparated asters would explain why the midzone complex-dependent furrows in TPXL-1–depleted embryos do not form until after the asters separate.

Aster-based Inhibition Refines Midzone-based Signaling to Confine Furrow Formation to a Unique Site

Preventing aster separation, by simultaneously inhibiting TPXL-1 and Gα signaling-based cortical forces pulling on the asters, leads to an increased delay followed by the simultaneous formation of multiple furrows that ingress to-

ward the midzone. We explain this result by proposing that in addition to controlling furrow formation in a midzone-independent manner, astral inhibition also interacts with the midzone-based signal to limit furrow formation to a single site (Figure 9A, bottom row). The fact that unseparated asters do not prevent furrowing indefinitely suggests that the asters eventually lose the ability to inhibit cortical contractility (Figure 9B). Loss of this inhibition occurs ~4 min after anaphase onset, a time point after the completion of cytokinesis in control cells. We favor a model in which the separated asters limit furrow formation to a unique site by spatially restricting the region of the cortex where contractile ring proteins are able to accumulate in response to the midzone-based signal (Figure 9, A and B). In the absence of inhibition by the asters, midzone signaling generates a broad contractile region, and multiple furrows form and ingress toward the midzone simultaneously. The idea that inhibition by the asters provides spatial information that refines midzone-based signaling is consistent with a recent study in sea urchin embryos in which increased levels of activated myosin II were observed over a substantially broader region of the equatorial cortex when astral microtubules were partially depolymerized by low dose nocodazole treatment (Foe and von Dassow, 2008).

In the model we propose, aster-based inhibition is a constant that acts throughout cytokinesis. Initially, aster-based inhibition patterns anaphase onset triggered contractility to prime the equatorial cortex for ingression and to promote the formation of an initial furrow. Later, aster-based inhibition confines the midzone-based signal to the equatorial plane to limit furrow ingression to a single site. Our model differs from the model of Bringmann and Hyman (2005), who proposed that the asters and midzone provide sequential redundant positive signals, in two key respects. In our model the asters are inhibitory; they modulate contractile signals but do not generate them on their own. In addition, the aster and midzone signals in our model function together rather than being functionally redundant, because the midzone-based signal requires input from aster-based inhibition to confine its action to a unique site.

ACKNOWLEDGMENTS

We thank Rebecca Green, Julie Canman, Amy Maddox, Ana Carvalho, and Chris Campbell for critical reading of the manuscript and Yuji Kohara (National Institute of Genetics, Mishima, Japan) for gene-specific cDNAs. K. O. and A. D. receive salary and additional support from the Ludwig Institute for Cancer Research. K. O. was a Pew Scholar in the Biomedical Sciences. L. L. was supported by the National Institutes of Health/National Institute of General Medical Sciences funded University of California, San Diego Genetics Training Program (T32 GM008666) and a training grant from the National Cancer Institute.

REFERENCES

Audhya, A., Hyndman, F., McLeod, I. X., Maddox, A. S., Yates, J. R., 3rd, Desai, A., and Oegema, K. (2005). A complex containing the Sm protein CAR-1 and the RNA helicase CGH-1 is required for embryonic cytokinesis in *Caenorhabditis elegans*. J. Cell Biol. *171*, 267–279.

Bringmann, H., Cowan, C. R., Kong, J., and Hyman, A. A. (2007). LET-99, GOA-1/GPA-16, and GPR-1/2 are required for aster-positioned cytokinesis. Curr. Biol. *17*, 185–191.

Bringmann, H., and Hyman, A. A. (2005). A cytokinesis furrow is positioned by two consecutive signals. Nature *436*, 731–734.

Canman, J. C., Hoffman, D. B., and Salmon, E. D. (2000). The role of pre- and post-anaphase microtubules in the cytokinesis phase of the cell cycle. Curr. Biol. *10*, 611–614.

Chen, W., Foss, M., Tseng, K., and Zhang, D. (2008). Redundant mechanisms recruit actin into the contractile ring in silkworm spermatocytes. PLoS Biol. *6*, e209.

Dechant, R., and Glotzer, M. (2003). Centrosome separation and central spindle assembly act in redundant pathways that regulate microtubule density and trigger cleavage furrow formation. Dev. Cell *4*, 333–344.

Desai, A., Rybina, S., Muller-Reichert, T., Shevchenko, A., Shevchenko, A., Hyman, A., and Oegema, K. (2003). KNL-1 directs assembly of the microtubule-binding interface of the kinetochore in *C. elegans*. Genes Dev. *17*, 2421–2435.

Eggert, U. S., Mitchison, T. J., and Field, C. M. (2006). Animal cytokinesis: from parts list to mechanisms. Annu. Rev. Biochem. *75*, 543–566.

Foe, V. E., Field, C. M., and Odell, G. M. (2000). Microtubules and mitotic cycle phase modulate spatiotemporal distributions of F-actin and myosin II in *Drosophila* syncytial blastoderm embryos. Development *127*, 1767–1787.

Foe, V. E., and von Dassow, G. (2008). Stable and dynamic microtubules coordinately shape the myosin activation zone during cytokinetic furrow formation. J. Cell Biol. *183*, 457–470.

Francis-Lang, H., Minden, J., Sullivan, W., and Oegema, K. (1999). Live confocal analysis with fluorescently labeled proteins. Methods Mol. Biol. *122*, 223–239.

Glotzer, M. (2004). Cleavage furrow positioning. J. Cell Biol. *164*, 347–351.

Glotzer, M. (2005). The molecular requirements for cytokinesis. Science *307*, 1735–1739.

Gönczy, P., and Rose, L. S. (2005). Asymmetric cell division and axis formation in the embryo. In *WormBook*, ed. The *C. elegans* Research Community, WormBook, doi/10.1895/wormbook. 1.30.1, http://www.wormbook.org.

Hannak, E., Kirkham, M., Hyman, A. A., and Oegema, K. (2001). Aurora-A kinase is required for centrosome maturation in *Caenorhabditis elegans*. J. Cell Biol. *155*, 1109–1116.

Jantsch-Plunger, V., Gönczy, P., Romano, A., Schnabel, H., Hamill, D., Schnabel, R., Hyman, A. A., and Glotzer, M. (2000). CYK-4, A Rho family GTPase activating protein (GAP) required for central spindle formation and cytokinesis. J. Cell Biol. *149*, 1391–1404.

Kaitna, S., Mendoza, M., Jantsch-Plunger, V., and Glotzer, M. (2000). Incenp and an aurora-like kinase form a complex essential for chromosome segregation and efficient completion of cytokinesis. Curr. Biol. *10*, 1172–1181.

Kozlowski, C., Srayko, M., and Nedelec, F. (2007). Cortical microtubule contacts position the spindle in *C. elegans embryos*. Cell *129*, 499–510.

Maddox, A. S., Lewellyn, L., Desai, A., and Oegema, K. (2007). Anillin and the septins promote asymmetric ingression of the cytokinetic furrow. Dev. Cell *12*, 827–835.

Maddox, A. S., and Oegema, K. (2003). Deconstructing cytokinesis. Nat. Cell Biol. *5*, 773–776.

Nance, J., Munro, E. M., and Priess, J. R. (2003). *C. elegans* PAR-3 and PAR-6 are required for apicobasal asymmetries associated with cell adhesion and gastrulation. Development *130*, 5339–5350.

Oegema, K., Desai, A., Rybina, S., Kirkham, M., and Hyman, A. A. (2001). Functional analysis of kinetochore assembly in *Caenorhabditis elegans*. J. Cell Biol. *153*, 1209–1226.

Oegema, K., and Mitchison, T. J. (1997). Rappaport rules: cleavage furrow induction in animal cells. Proc. Natl. Acad. Sci. USA *94*, 4817–4820.

Özlü, N., Srayko, M., Kinoshita, K., Habermann, B., O'Toole, E. T., Muller-Reichert, T., Schmalz, N., Desai, A., and Hyman, A. A. (2005). An essential function of the *C. elegans* ortholog of TPX2 is to localize activated aurora A kinase to mitotic spindles. Dev. Cell *9*, 237–248.

Portier, N., Audhya, A., Maddox, P. S., Green, R. A., Dammermann, A., Desai, A., and Oegema, K. (2007). A microtubule-independent role for centrosomes and aurora A in nuclear envelope breakdown. 2007. Dev. Cell *12*, 515–529.

Powers, J., Bossinger, O., Rose, D., Strome, S., and Saxton, W. (1998). A nematode kinesin required for cleavage furrow advancement. Curr. Biol. *8*, 1133–1136.

Raich, W. B., Moran, A. N., Rothman, J. H., and Hardin, J. (1998). Cytokinesis and midzone microtubule organization in *Caenorhabditis elegans* require the kinesin-like protein ZEN-4. Mol. Biol. Cell *9*, 2037–2049.

Rappaport, R. (1969). Aster-equatorial surface relations and furrow establishment. J. Exp. Zool. *171*, 59–68.

Schumacher, J. M., Golden, A., and Donovan, P. J. (1998). AIR-2, An Aurora/Ipl1-related protein kinase associated with chromosomes and midbody microtubules is required for polar body extrusion and cytokinesis in *Caenorhabditis elegans* embryos. J. Cell Biol. *143*, 1635–1646.

Severson, A. F., Hamill, D. R., Carter, J. C., Schumacher, J., and Bowerman, B. (2000). The aurora-related kinase AIR-2 recruits ZEN-4/CeMKLP1 to the mitotic spindle at metaphase and is required for cytokinesis. Curr. Biol. *10*, 1162–1171.

Shuster, C. B., and Burgess, D. R. (2002). Transitions regulating the timing of cytokinesis in embryonic cells. Curr. Biol. *12*, 854–858.

Srayko, M., Kaya, A., Stamford, J., and Hyman, A. A. (2005). Identification and characterization of factors required for microtubule growth and nucleation in the early *C. elegans* embryo. Dev. Cell *9*, 223–236.

Straight, A. F., Cheung, A., Limouze, J., Chen, I., Westwood, N. J., Sellers, J. R., and Mitchison, T. J. (2003). Dissecting temporal and spatial control of cytokinesis with a myosin II inhibitor. Science *299*, 1743–1747.

Teichmann, E. (1903). Über die Beziehung zwischen Astrosphären und Furchen: Experimentelle Untersuchungen am Seeigelei. Wilhelm Roux Arch. Entwickl. Mech. Org. *16*, 243–327.

Verbrugghe, K. J., and White, J. G. (2004). SPD-1 is required for the formation of the spindle midzone but is not essential for the completion of cytokinesis in *C. elegans* embryos. Curr. Biol. *14*, 1755–1760.

Verbrugghe, K. J., and White, J. G. (2007). Cortical centralspindlin and G alpha have parallel roles in furrow initiation in early *C. elegans* embryos. J. Cell Sci. *120*, 1772–1778.

Werner, M., Munro, E., and Glotzer, M. (2007). Astral signals spatially bias cortical myosin recruitment to break symmetry and promote cytokinesis. Curr. Biol. *17*, 1286–1297.

White, J. G., and Borisy, G. G. (1983). On the mechanisms of cytokinesis in animal cells. J. Theor. Biol. *101*, 289–316.

Wilson, E. B. (1928). The Cell in Development and Heredity, New York: The MacMillin Company.

Wolpert, L. (1960). The mechanics and mechanism of cleavage. Int. Rev. Cytol. *10*, 163–216.

Zhou, M., and Wang, Y. L. (2008). Distinct pathways for the early recruitment of myosin II and actin to the cytokinetic furrow. Mol. Biol. Cell *19*, 318–326.